ELSEVIER

Contents lists available at ScienceDirect

Journal of Molecular Spectroscopy

journal homepage: www.elsevier.com/locate/yjmsp





The 130–500 GHz rotational spectroscopy of cyanopyrazine (C₄H₃N₂-CN)

Brian J. Esselman, Maria A. Zdanovskaia, Houston H. Smith, R. Claude Woods, Robert J. McMahon

Department of Chemistry, University of Wisconsin-Madison, Madison, WI 53706, USA

ARTICLE INFO

Keywords: Rotational spectroscopy Coriolis coupling Interstellar molecule Astrochemistry

ABSTRACT

The rotational spectrum of cyanopyrazine (2-pyrazinecarbonitrile, p- C_4 H₃N₂-CN) has been obtained from 130 to 500 GHz. Rotational transitions of cyanopyrazine have been measured, assigned, and least-squares fit for the first time. Over 7000 transitions of the ground vibrational state have been least-squares fit to partial octic, A- and S-reduced Hamiltonians with low statistical uncertainty ($\sigma_{\rm fit}=34$ kHz). Similar to other cyanoarenes, the first two fundamental modes are the out-of-plane (ν_{27} , A'') and in-plane (ν_{19} , A') nitrile bending modes, which form an a- and b-axis Coriolis-coupled dyad. Greater than 5800 transitions from each of these vibrational modes were fit to a partial octic, A-reduced Hamiltonian ($\sigma_{\rm fit}=38$ kHz), and the analysis reveals the precise energy separation, $\Delta E_{27,19}$, between the coupled vibrational states, as well as values for eight a- and b-type Coriolis-coupling coefficients, G_a , G_a^J , G_a^K , G_a^{JJ} , F_{bc}^K , G_b , G_b^J , and F_{ac} . Cyanopyrazine is a strongly polar derivative of pyrazine, thus cyanopyrazine can serve as a potential tracer molecule for its nonpolar parent compound in extraterrestrial environments. The transition frequencies and spectroscopic constants provided in this work, combined with theoretical or experimental nuclear quadrupole coupling constants, provide the foundation for future radio-astronomical searches for cyanopyrazine.

1. Introduction

The feasibility of radioastronomical detection of a molecule depends upon its population in the source of interest and on the intrinsic intensity of its rotational transitions due to its dipole moment. The direct detections of benzene [1] and other nonpolar species [1,2] in extraterrestrial environments rely upon infrared spectroscopy, but can be supported or suggested by detection of their polar, substituted derivatives by radioastronomy. The recent radioastronomical detections of benzonitrile [3] and two cyanonaphthalenes [4] not only provide confirmation of these species in the interstellar medium (ISM), but also suggest the presence of their parent species, benzene and naphthalene. The presence of these nitrile-substituted aromatic molecules and the many other nitrile-containing organic species in the ISM [5-7] inspired the recent rotational spectral analyses of several nitrile-containing heteroaromatic compounds (Fig. 1) by our group, including benzonitrile [8,9], 3-cyanopyridine [10], and 4-cyanopyridine [11] up to 360 GHz in their ground and vibrationally excited states. Similarly inspired, McNaughton et al. reported the 2 to 100 GHz spectroscopy of several polycyclic aromatic nitriles (1-cyanonaphthalene, 2-cyanonaphthalene, 9-cyanoanthracene, and 9-cyanophenanthrene) [12]. To facilitate

astronomical searches for additional cyanoarenes, we have measured the laboratory rotational spectra of cyanopyrazine (presented in this work), 2-cyanopyridine [13], and 2-cyanopyrimidine [14].

Unlike its isomeric dinitrogen-containing benzene analogues, pyridazine ($\mu_q = 4.22 \,\mathrm{D}$ [15]) and pyrimidine ($\mu_q = 2.334 \,\mathrm{D}$ [16]), pyrazine $(D_{2h}, \mu = 0)$ does not possess a permanent dipole moment due to the para relationship of the nitrogen atoms and cannot be the direct target of a radioastronomical search. While neither pyridazine nor pyrimidine has been detected in the ISM [17-20], and both molecules are part of a larger dilemma regarding the apparent absence of aromatic heterocycles in the list of organic molecules in the ISM, pyrazine represents an intriguing possibility as an astrochemical species. Pyrazine is nearly isoenergetic with pyrimidine, both of which are 19.7 kcal/mol more stable than pyridazine [21-23]. Due to its lack of a permanent dipole moment, tracer molecules are required to explore the potential contribution of pyrazine to interstellar organic chemistry. Substituted pyrazines have not garnered significant attention in the spectroscopy community. Transition frequencies and rotational constants have been provided for chloropyrazine [24,25], but not for other substituted pyrazines. Given the prevalence of organic nitriles in the ISM, cyanopyrazine is an ideal tracer molecule for pyrazine. Detection of any

E-mail addresses: rcwoods@wisc.edu (R.C. Woods), robert.mcmahon@wisc.edu (R.J. McMahon).

^{*} Corresponding authors.

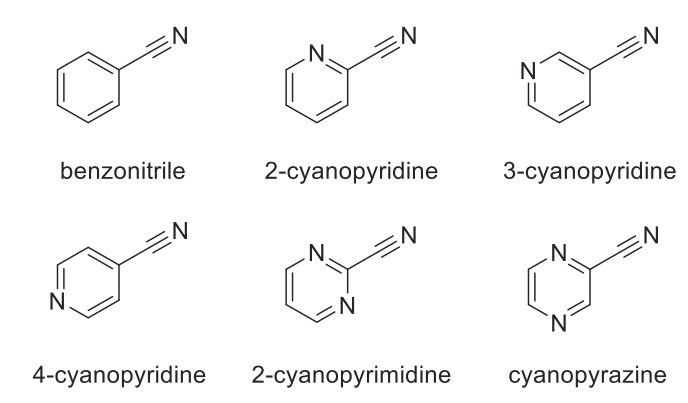


Fig. 1. Cyanoarenes derived from benzene, pyridine, pyrimidine, and pyrazine.

Table 1Energy differences between out-of-plane and in-plane nitrile bending modes for cyanoarenes.

	out-of-plane	in-plane	$\Delta E \text{ (cm}^{-1}\text{)}$
benzonitrile [8,9] 3-cyanopyridine [10]	$ u_{22}, B_1 \nu_{30}, A'' $	$\nu_{33}, B_2 \\ \nu_{21}, A'$	19.1081701(74) 15.7524693 (37)
4-cyanopyridine [11]	ν_{20}, B_1	ν_{30}, B_2	18.806554 (11)

heterocycle or substituted heterocycle in the ISM would represent a dramatic breakthrough for the field [17–20], because derivatives of the parent aromatic compounds are ubiquitous in biologically relevant molecules. Alkylated pyrazines are found in various natural sources, including coffee beans, cocoa beans, and vegetables and are produced by insects, fungi, and bacteria [26].

The two lowest-energy vibrational modes of the cyanoarenes are typically the out-of-plane and in-plane nitrile bending modes, which are often sufficiently close in energy to observe Coriolis coupling between them at millimeter-wave frequencies. Analysis of the rotational spectra for these vibrational modes for benzonitrile [8,9], 3-cyanopyridine [10], and 4-cyanopyridine [11] provided highly accurate and precise relative energy values, Table 1. The Coriolis coupling and resultant state mixing necessitate that transitions of the vibrational modes are least-squares fit as a Coriolis-coupled dyad. It is this interaction that results in numerous resonant transitions and coupling-allowed, nominal interstate transitions that provide the accurate and precise vibrational energy spacing. Only for benzonitrile have the precise band origins of each mode been measured by high-resolution infrared spectroscopy [9]. Herein, we report the rotational spectroscopy and analysis of the ground and two

lowest-energy vibrationally excited states of cyanopyrazine from $130\ \mathrm{to}$ 500 GHz.

2. Experimental methods

A commercial sample of cyanopyrazine was used without further purification for all spectroscopic measurements. The rotational spectrum was collected using a millimeter-wave spectrometer that has been previously described [27,28] in the 130 to 230 and 235 to 360 GHz frequency ranges, in a continuous flow at room temperature, with sample pressures of 3 to 12 mTorr. Additional spectral data were obtained with a newly acquired amplification and multiplication chain that extends the frequency range to 500 GHz. The separate spectral segments were combined into a single broadband spectrum using Kisiel's Assignment and Analysis of Broadband Spectra (AABS) software [29,30]. The complete spectrum from 130 to 500 GHz was obtained automatically over approximately nine days using the following experimental parameters: 0.045 kHz frequency increment, 0.6 MHz/s sweep rate, 10 ms time constant, and 50 kHz AM and 500 kHz FM modulation in a tone-burst design. Pickett's SPFIT/SPCAT [31] were used for leastsquares fits and spectral predictions, along with Kisiel's PIFORM, PLANM, and AC programs for analysis [32]. A uniform frequency measurement uncertainty of 0.050 MHz was assumed for all measurements.

3. Computational methods and results

Electronic structure calculations were carried out with Gaussian 16 [33] using the WebMO interface [34] to obtain theoretical spectroscopic constants. Optimized geometries at the B3LYP/6-311+(2d,p) and MP2/

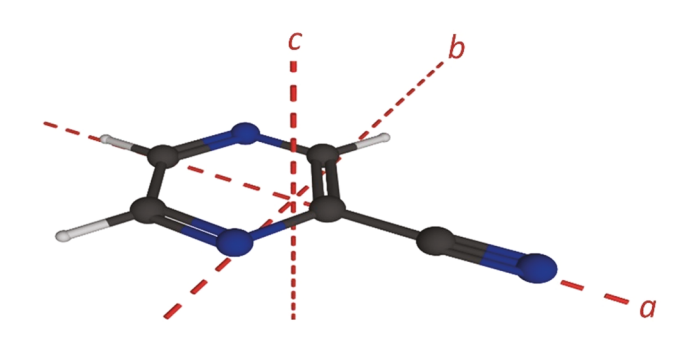


Fig. 3. Cyanopyrazine (C_s , $\mu_a = 4.2$ D, $\mu_b = 0.1$ D, B3LYP) structure with principal inertial axes.

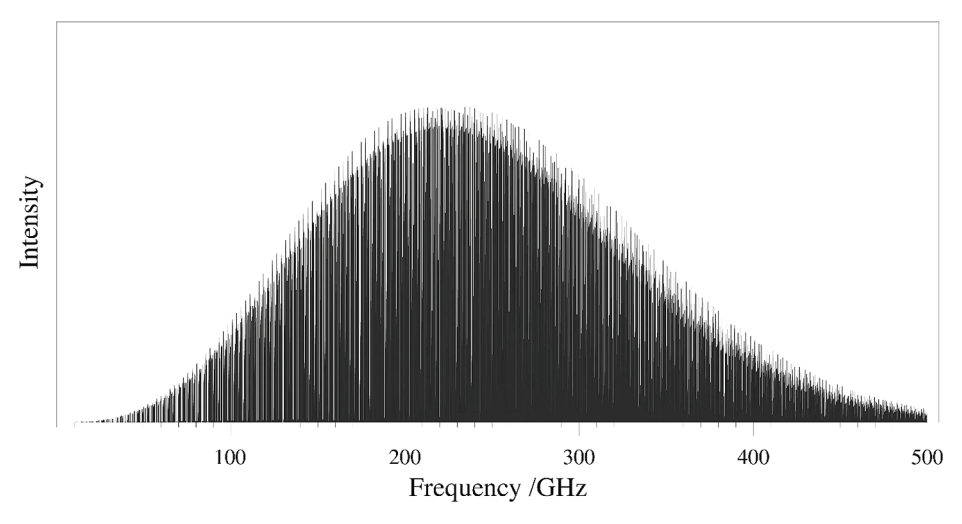


Fig. 2. Predicted spectrum (SPCAT) of the ground vibrational state of cyanopyrazine at 292 K.

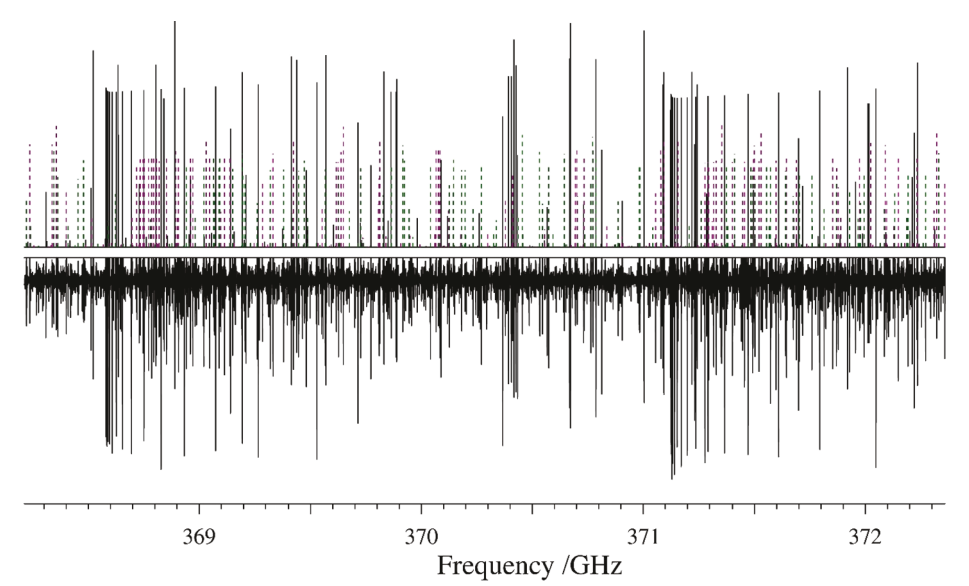


Fig. 4. Predicted (top) and experimental (bottom) rotational spectra of cyanopyrazine from 368.2 to 372.4 GHz. Ground-state cyanopyrazine with prominent transitions for the J''+1=144 and J''+1=145 bands appear in black. Transitions for ν_{27} are in purple and transitions for ν_{19} are in dark green. Unassigned transitions are attributable to other vibrationally excited states of cyanopyrazine. (For interpretation of the references to colour in this figure legend, the reader is referred to the web version of this article.)

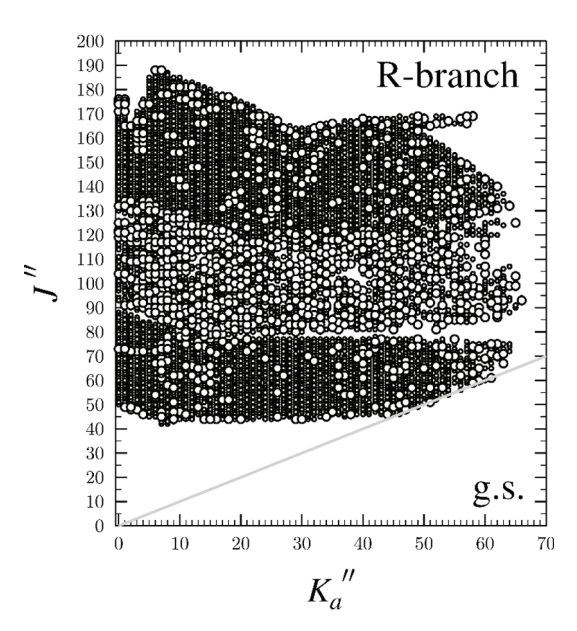


Fig. 5. Data distribution plot for the least-squares fit of spectroscopic data for the vibrational ground state of cyanopyrazine. The size of the symbol is proportional to the value of $|(f_{obs.} - f_{calc.})/\delta f|$, where δf is the frequency measurement uncertainty, and all values are smaller than 3.

6-311+(2d,p) levels of theory were obtained using "verytight" convergence criteria and an "ultrafine" integration grid, and subsequent anharmonic vibrational frequency calculations were carried out using second-order vibrational perturbation theory (VPT2). All computational output files can be found in the supplemental material.

4. Cyanopyrazine rotational spectra

The recently expanded frequency range of our instrument allowed us to measure the spectrum of cyanopyrazine up to 500 GHz, a frequency coverage beyond that used in previous works on cyanoarenes (up to 375 GHz) [8–11]. This range is nearly optimal for cyanopyrazine at the ambient laboratory temperature (Fig. 2), as it covers the most intense transitions based upon the rotational populations. The expanded frequency coverage was also advantageous for the least-squares fitting of ν_{27} and ν_{19} , due to the high J''+1 values of the most intense transitions

of these vibrationally excited states (*vide infra*). The relatively low value of C_0 (\sim 1276 MHz) for all cyanopyrazine vibrational states results in the $K_a=0$ series transition near 130 GHz having a value of J''+1=51 and increasing to J''+1=195 just below 500 GHz. This range of J''+1 (and the resulting range of K_a) quantum numbers provides a wealth of spectroscopic information on the centrifugal distortion and necessitates a high-order Hamiltonian to adequately model the spectrum.

4.1. Ground-state spectral analysis

The ground-state spectrum of cyanopyrazine ($\mu_a = 4.2 \text{ D}, \mu_b = 0.1 \text{ D},$ B3LYP; $\kappa = -0.854$) has not been reported, despite this benzonitrile analog being commercially available. The strong electron-withdrawing effect of the nitrile group results in a dipole moment nearly coincidental with that substituent (Fig. 3) and the a principal axis. Due to the asymmetry of the ring caused by the nitrile substitution, there is also a slight b-axis dipole component. The large difference in the a- and b-axis dipole components results in a-type transitions that are roughly 2000 times more intense than the *b*-type transitions. As a result, the rotational spectrum of cyanopyrazine is dominated by intense ^aR_{0.1} transitions across the frequency range (Fig. 4). Despite being a prolate molecule, cyanopyrazine and other substituted arenes [8-11,35] have prominent oblate-type bands, in which transitions in the bands begin at $K_a = 0$ and increase in K_a as frequency increases. Cyanopyrazine displays prolatetype bands at high K_a , though the spacing and intensity make them much less prominent. The much weaker Q-branch transitions could not be observed and assigned for cyanopyrazine owing to the spectral density created by excited vibrational states of cyanopyrazine. Thus, the final transition data set for the ground vibrational state contained only atype, R-branch transitions. As shown in Fig. 5, these transitions cover a broad range of quantum numbers, including J'' + 1 = 42 to 189 and $K_a =$ 0 to 66. The spectral density and frequency range investigated allowed for the measurement, assignment, and least-squares fitting of 7078 independent transition frequencies to partial octic, A- and S-reduced Hamiltonians with low error ($\sigma_{fit} = 34$ kHz). The resulting spectroscopic constants are reported in Table 2, along with their corresponding computed values. Though several octic terms are required in the A and S reduction least-squares fits, no readily available computational software is able to provide these values for comparison. Thus, L_K and the offdiagonal octic terms that could not be satisfactorily determined were held at values of zero in the least-squares fitting.

The B3LYP-computed rotational constants are in excellent agreement with the experimental values, similar to that seen for 3- and 4-

Table 2Experimental and computational spectroscopic constants for the ground vibrational state of cyanopyrazine (S- and A-reduced Hamiltonians, I^r representation).

	S reduction, I ^r representation			A reduction, I ^r representation			
	Experimental	B3LYP ^a	MP2 ^a		Experimental	B3LYP ^a	MP2 ^a
A ₀ (MHz)	6003.12984 (58)	6016.1	5950.4	A_0 (MHz)	6003.12822 (58)	6016.1	5950.4
B_0 (MHz)	1621.517450 (24)	1619.4	1605.5	B_0 (MHz)	1621.518806 (24)	1619.4	1605.5
C_0 (MHz)	1276.428481 (25)	1276.7	1264.1	C_0 (MHz)	1276.427155 (25)	1276.7	1264.1
D_J (kHz)	0.0359497 (18)	0.0348	0.0345	Δ_J (kHz)	0.0492594 (19)	0.0471	0.0472
D_{JK} (kHz)	1.182301 (25)	1.11	1.15	Δ_{JK} (kHz)	1.102415 (24)	1.04	1.07
D_K (kHz)	0.2897 (13)	0.317	0.282	Δ_K (kHz)	0.3525 (13)	0.379	0.345
d_1 (kHz)	-0.01183021 (59)	-0.0112	-0.0113	δ_J (kHz)	0.01182909 (60)	0.0112	0.0113
d_2 (kHz)	-0.00665773 (39)	-0.00616	-0.00636	δ_K (kHz)	0.702668 (42)	0.660	0.677
H_J (Hz)	-0.000014359 (71)	-0.0000123	-0.0000135	Φ_J (Hz)	0.000001797 (74)	0.00000275	0.00000306
H_{JK} (Hz)	0.0013660 (16)	0.00117	0.00129	Φ_{JK} (Hz)	0.0019713 (18)	0.00170	0.00185
H_{KJ} (Hz)	-0.007530 (15)	-0.00646	-0.00718	Φ_{KJ} (Hz)	-0.009803 (15)	-0.00845	-0.00932
H_K (Hz)	0.01171 (81)	0.00594	0.00652	Φ_K (Hz)	0.01097 (83)	0.00738	0.00807
h_1 (Hz)	0.000000244 (14)	-0.000000153	-0.000000148	ϕ_J (Hz)	0.000001844 (15)	0.00000129	0.00000142
h_2 (Hz)	0.000008265 (11)	0.00000756	0.00000829	ϕ_{JK} (Hz)	0.0009204 (11)	0.000864	0.000945
h_3 (Hz)	0.0000016326 (42)	0.00000145	0.00000156	ϕ_K (Hz)	0.009580 (31)	0.00862	0.00925
L_J (mHz)	0.0000000295 (10)			L_J (mHz)	0.0000000361 (10)		
L_{JJK} (mHz)	-0.000002512 (15)			L_{JJK} (mHz)	-0.000002972 (15)		
L_{JK} (mHz)	0.00002268 (18)			L_{JK} (mHz)	0.00001795 (19)		
L_{KKJ} (mHz)	-0.0001332 (26)			L_{KKJ} (mHz)	-0.0001153 (26)		
L_K (mHz)	[0.]			L_K (mHz)	[0.]		
$\Delta_i (u \mathring{A}^2)^{b,c}$	0.075770 (12)			$\Delta_i (u \mathring{A}^2)^{b,c}$	0.076419 (12)		
$N_{ m lines}$ d	7078			$N_{ m lines}$ d	7078		
σ _{fit} (MHz)	0.034			σ _{fit} (MHz)	0.034		

^a Evaluated with the 6-311+G(2d,p) basis set.

^d Number of fitted transition frequencies.

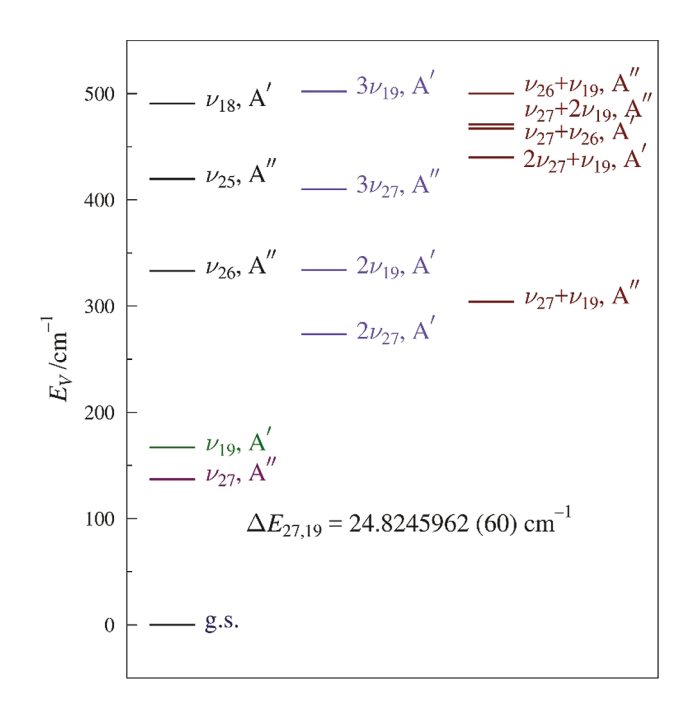


Fig. 6. Vibrational energy levels of cyanopyrazine below 500 cm $^{-1}$ from computed fundamental frequencies (B3LYP/6-311+G(2d,p)). The value of $\Delta E_{27,19}$ results from the experimental perturbation analysis of ν_{27} and ν_{19} in this work

cyanopyridine [10,11]. The largest discrepancy between the experimental and computed rotational constant values is for A_0 , which is overestimated by 13 MHz (0.21%). The B3LYP values of B_0 and C_0 are within 2.1 MHz and 0.3 MHz of their experimental values, respectively. All of the B3LYP quartic centrifugal distortion constants are in good agreement (within 10% of their experimental values) in both reductions. There is much poorer agreement between the computed sextic distortion

constants and the experimental values, typically varying from 6 to 30%. Both Φ_I and H_K , however, differ by about 50% from their computed values, while h_1 is the wrong sign. At first glance, it appears that the MP2 computed values are worse than their B3LYP counterparts. Though the agreement of the MP2 values is inferior for the rotational constants, the deviations from the experimental values all remain less than 1%. For nearly all of the remaining spectroscopic constants, the MP2 value is closer to the experimental value than the B3LYP-computed value. All of the MP2 quartic centrifugal distortion constants are within 5% of their experimental values, and all of them show better agreement than the B3LYP values. With regard to the sextic centrifugal distortion constants, the general agreement of the MP2-computed constants is between 0.2 and 6%. The exceptions are Φ_J , Φ_K , ϕ_J , H_K , and h_1 , with large discrepancies of 70%, -26%, -23%, -44%, and -160%, respectively. As with the B3LYP value of h_1 , its MP2 value has the incorrect sign. Despite the issues with both sets of computed spectroscopic constants, both B3LYP and MP2 values provide a priori predictions of the rotational spectrum of cyanopyrazine sufficient to identify and assign its transitions in the experimental spectrum.

4.2. Spectral analysis of ν_{27} and ν_{19}

Similar to other cyanoarenes [8–11], the first two fundamental modes of cyanopyrazine are the out-of-plane and in-plane nitrile bending modes, ν_{27} and ν_{19} , respectively. These two vibrational states form a Coriolis-coupled dyad that is well separated in energy from the ground state and the next vibrationally excited state, $2\nu_{27}$. The previous low-resolution infrared (IR) spectroscopy of cyanopyrazine provides an assignment of most of the cyanopyrazine vibrational modes [36–39], though there is some ambiguity about the assignment of the modes at 160, 173, and 339 cm⁻¹, with both of the lower modes assigned A' symmetry [38]. The two lowest-frequency modes, ν_{27} (A'') and ν_{19} (A'), are predicted to have energies of 137 and 167 cm⁻¹ (B3LYP) or 136 and 162 cm⁻¹ (MP2). It is likely that the mode at 339 cm⁻¹, designated A' in the solution phase IR and Raman vibrational study, is ν_{26} (A''), but it is not clear whether either of the modes observed at 160 and 173 cm⁻¹ are ν_{27} (A'') or ν_{19} (A'). As a result of that ambiguity, the vibrational state

^b Inertial defect, $\Delta_i = I_c - I_a - I_b$.

 $^{^{\}mathrm{c}}$ Calculated using PLANM from the B_0 constants.

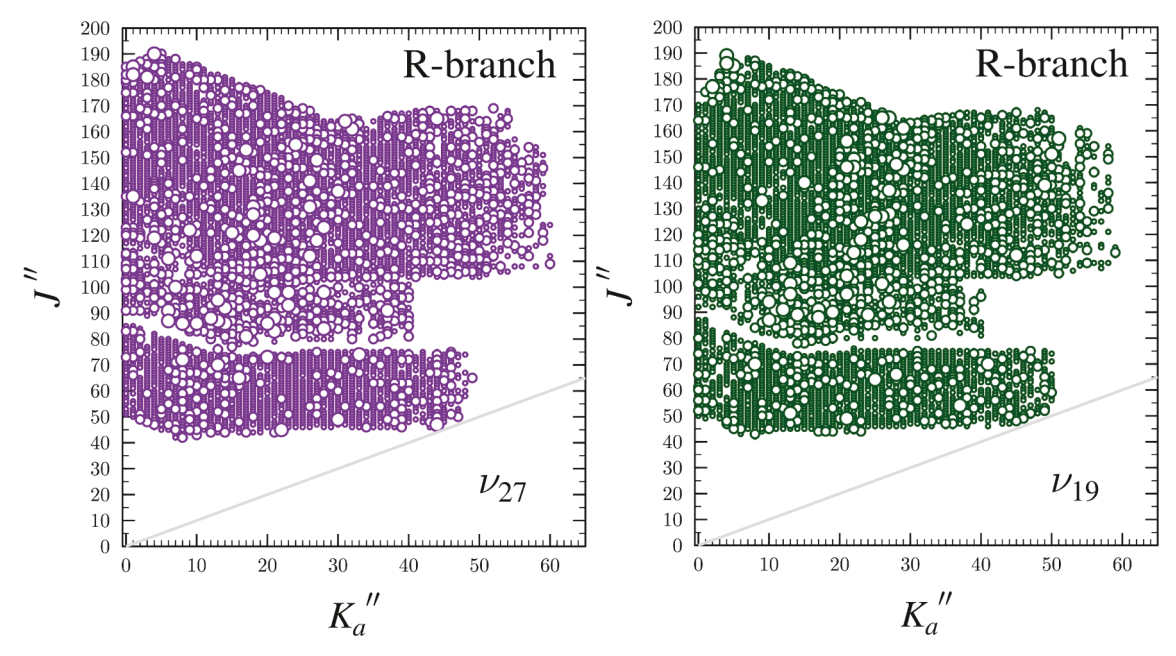


Fig. 7. Data distribution plots for the least-squares fit of spectroscopic data for the lowest-energy fundamental states of cyanopyrazine, ν_{27} (purple) and ν_{19} (dark green). The size of the symbol is proportional to the value of $|(f_{obs.} - f_{calc.})/\delta f|$, where δf is the frequency measurement uncertainty, and all values are smaller than 3. (For interpretation of the references to colour in this figure legend, the reader is referred to the web version of this article.)

diagram shown Fig. 6. is based upon the computed (B3LYP) fundamental frequencies. The initial predictions for these vibrational states were based upon the experimental ground-state rotational constants, computational vibration-rotation interaction constants, and the groundstate centrifugal distortion constants. After initial measurement, assignment, and least-squares fitting of these fundamental states, it became clear that a single-state Hamiltonian was insufficient to model their rotational spectra. To address this problem, a Coriolis-coupled dyad Hamiltonian was employed similar to our previous works [8–11,35,40,41]. The A'' and A' symmetries of these states allow both α and b-axis Coriolis coupling. Thus, initially, computed G_a , G_b , and $\Delta E_{27,19}$ values were added to the least-squares fit. As transitions were added to the fit, these parameters were allowed to vary, and additional parameters were included until the available transitions could be modeled adequately. The breadth of transitions is shown in Fig. 7, and the resulting spectroscopic constants are provided in Table 3.

The final least-squares fit of the Coriolis-coupled dyad (ν_{27} and ν_{19}) contained over 12,000 transitions, including many transitions involving energy levels perturbed by the coupling, many intensely shifted resonant transitions created by nearly degenerate energy levels of ν_{27} and ν_{19} , and 37 formally forbidden, coupling-allowed, nominal interstate transitions. Due to the intensity of the transitions for each vibrationally excited state, the number of transitions for each state in the final data set for v_{27} and ν_{19} (6257 and 5893, respectively) is decreased only slightly from that of the ground state (7078). In the frequency range studied, the observed transitions range from 42 to 191 in J''+1 and from 0 to 60 in K_a . Since many of the intense resonant transitions and nominal interstate transitions occur beyond 360 GHz, extending the measured spectral range to 500 GHz was an important factor in obtaining a satisfactory least-squares fit. Data from the higher frequency range had not been necessary in previous works on analogous species [8-11] and can be attributed to the larger energy difference between the coupled states in cyanopyrazine, relative to the previously studied compounds (Table 1).

In cyanopyrazine, the energy separation between ν_{27} and ν_{19} ($\Delta E_{27,19} =$ 24.8245962 (60) cm⁻¹) requires higher values of J and K for the energy levels of ν_{27} to approach those of ν_{19} closely enough to create resonances (vide infra). It is important to note that this energy difference varies substantially from the frequencies reported for the two lowest-energy fundamentals in the previously reported low-resolution IR and Raman spectroscopic data [38] of 173 and 160 cm⁻¹, casting doubt on the previous liquid-phase IR assignments. In addition to determining a highly accurate and precise $\Delta E_{27,19}$ value, the least-squares fit provides a nearly complete set of spectroscopic constants of a sextic centrifugally distorted, A-reduced Hamiltonian (excluding the off-diagonal terms ϕ_{JK} and ϕ_K) and eight Coriolis-coupling coefficients $(G_a, G_a^J, G_a^K, G_a^{JJ}, F_{bc}^K, G_b,$ G_b^J , and F_{ac}). Attempts to include F_{bc} in the least-squares fit were made, but were not successful. In view of that result, we found it surprising that F_{bc}^{K} was necessary to achieve a reasonable fit and could be well determined.

The computed spectroscopic constants B_v and C_v are in quite close agreement with their experimentally determined values (Table 4). At both the MP2 and B3LYP levels, the predicted vibration-rotation interaction constants $(B_0 - B_v)$ differ by less than 10% from their experimental values, with the MP2 values in slightly closer agreement than the B3LYP values. The very close agreement seen for the B_0 – B_{ν} values provides evidence that the deperturbation of the constants in the computational results and the treatment of the Coriolis-coupling were both reasonably effective. For the A_0 – A_{ν} values, however, there is a very large discrepancy between the computed and experimental values. At both levels of theory, the magnitudes of the $A_0 - A_{\nu}$ values are computed to be five or six times larger than the experimental values. This is largely due to residual Coriolis coupling in the computed values, given the very large magnitudes of the values and the smaller magnitudes of the experimental $A_0 - A_v$ values in this and similar works. The B3LYP-predicted values are slightly closer to the experimental ones than the MP2 values, in this case. Given the fairly large experimental A_0-A_{ν}

Table 3Experimentally determined parameters for the ground state and vibrationally excited states 27 and 19 of cyanopyrazine (A-reduced Hamiltonian, I^r representation).

	ground state ^a	ν ₂₇ (A", 136 cm ⁻¹) ^{a,b}	$v_{19} (A', 162 \text{ cm}^{-1})^{a,b}$	
A_{ν} (MHz) B_{ν} (MHz) C_{ν} (MHz)	6003.12822 (58) 1621.518806 (24) 1276.427155 (25)	6026.492 (18) 1623.29554 (16) 1278.422236 (28)	5977.166 (18) 1624.75111 (17) 1277.400270 (27)	
Δ_{J} (kHz) Δ_{JK} (kHz) Δ_{K} (kHz) δ_{J} (kHz) δ_{K} (kHz)	0.0492594 (19) 1.102415 (24) 0.3525 (13) 0.01182909 (60) 0.702668 (42)	0.05013381 (98) 1.12777 (17) 0.3421 (28) 0.01191174 (61) 0.704032 (38)	0.0504064 (10) 1.05278 (17) 0.4081 (42) 0.01227503 (66) 0.706581 (29)	
$ \Phi_{J}(Hz) $ $ \Phi_{JK}(Hz) $ $ \Phi_{KJ}(Hz) $ $ \Phi_{K}(Hz) $ $ \phi_{J}(Hz) $	0.000001797 (74) 0.0019713 (18) -0.009803 (15) 0.01097 (83) 0.000001844 (15) 0.0009204 (11) 0.009580 (31)	0.000002534 (20) 0.0020104 (37) -0.0104488 (91) 0.00672 (61) 0.000002043 (12) [0.0009204] [0.009580] 744222.6 24.8	0.000002850 (20) 0.0018932 (37) -0.008731 (12) 0.00602 (53) 0.000002359 (14) [0.0009204] [0.009580] 7 (18) 245962 (60)	
G_a (MHz) G_a^J (MHz) G_a^K (MHz) G_a^{M} (MHz) G_b^J (MHz) G_b^J (MHz) G_b^J (MHz) G_b^J (MHz) G_b^J (MHz)		10789.33 (63) -0.0052515 (62) -0.029393 (77) 0.00000000517 (11) -0.00001287 (20) -134.02 (45) 0.0000378 (12) -1.079 (12)		
$egin{aligned} arDelta_i \left(ext{u} ext{Å}^2 ight)^c \ N_{ ext{lines}}^{e} \ oldsymbol{\sigma}_{ ext{fit}} \left(ext{MHz} ight) \end{aligned}$		0.012604 (26) 6257 0.038	0.02917 (26) 5893 0.037	

^a Octic centrifugal distortion constants not shown and held constant at their ground-state values in Table 2.

values, it is possible that they also retain untreated Coriolis coupling, though to a much lesser extent than the computed values. The MP2 $E_{27,19}$ value of 26.4 cm 1 is in excellent agreement with the very precise experimental value, while the B3LYP value is an overestimate by 6 cm 1 . The Coriolis $^{x}_{27\,19}$ values show very good agreement between theory and experiment at the B3LYP and MP2 levels of theory, which, combined with the low $_{\rm fit}$ value, indicates a satisfactory treatment of the a-axis and b-axis Coriolis coupling in the least-squares fit.

Further evidence of an adequate treatment of the dyad by the Hamiltonian model is the ability to include many resonant and nominal interstate transitions in the data set, whose prediction is heavily dependent on the $E_{27,19}$ value and Coriolis-coupling constants. Sharp a-type and b-type resonances are observed due to mixing of $_{27}$ and $_{19}$ energy levels that are nearly degenerate, as shown in Fig. 8. A minus superscript on the K_a value indicates that K_a K_c J 1, whereas a plus superscript indicates that K_a K_c J At J 1 157, there is an

intense a-type resonance between $_{27}$ and $_{19}$ with a K_a 2 selection rule. The resonant transitions are displaced from their unperturbed transition frequencies by about 1.5 GHz. There are additional small resonances in the K_a 16 series of 19 that correspond to resonances in different 27 series. Each of these series displays the large undulations due to centrifugal distortion and Coriolis coupling between these states. Fig. 9 shows how these resonances and undulations progress across the K_a series of $_{27}$. The undulations and resonances become more pronounced and move to progressively higher J 1 values as a function of K_a . While it is generally possible to obtain quartic distortion constants and preliminary values of the energy difference and Coriolis-coupling constants from the undulations, many local resonances are often needed to obtain precise determinations of the latter constants. The resonance progression plot shows that, for cyanopyrazine, most of the intense resonances occur after J=1 100, reiterating the importance of obtaining the higher-frequency data (360 500 GHz) used in this

^b Fundamental frequencies calculated using MP2/6-311+G(2d,p).

^c Inertial defect, $\Delta_i = I_c - I_a - I_b$.

^d Calculated using PLANM from the B_0 constants.

^e Number of fitted transition frequencies.

Table 4Vibration-rotation interaction and Coriolis-coupling constants of cyanopyrazine.

	Experimental	B3LYP ^a	MP2 ^a
$A_0 - A_{27}$ (MHz)	-23.364 (18)	112.0	138.7
$B_0 - B_{27}$ (MHz)	-1.77673(17)	-1.71	-1.66
$C_0 - C_{27}$ (MHz)	-1.995081(37)	-1.97	-1.92
$A_0 - A_{19}$ (MHz)	25.962 (18)	-109.5	-136.4
$B_0 - B_{19}$ (MHz)	-3.23230(17)	-3.07	-3.18
$C_0 - C_{19}$ (MHz)	-0.973115(37)	-0.90	-0.95
$\frac{(A_0 - A_{27}) + (A_0 - A_{19})}{2}$ (MHz)	1.299 (13)	1.29	1.14
$\frac{(B_0-B_{27})+(B_0-B_{19})}{2}$ (MHz)	-2.50452 (12)	-2.39	-2.42
$\frac{(C_0 - C_{27}) + (C_0 - C_{19})}{2}$ (MHz)	-1.484098 (26)	-1.43	-1.44
$\left \zeta_{27,19}^a\right $	0.899	0.804	0.808
$\left \zeta_{27,19}^{b}\right $	0.0413	0.036	0.037
$\Delta E_{27,19} \text{ (cm}^{-1})$	24.8245962 (60)	30.6	26.4

^aEvaluated with the 6-311+G(2d,p) basis set.

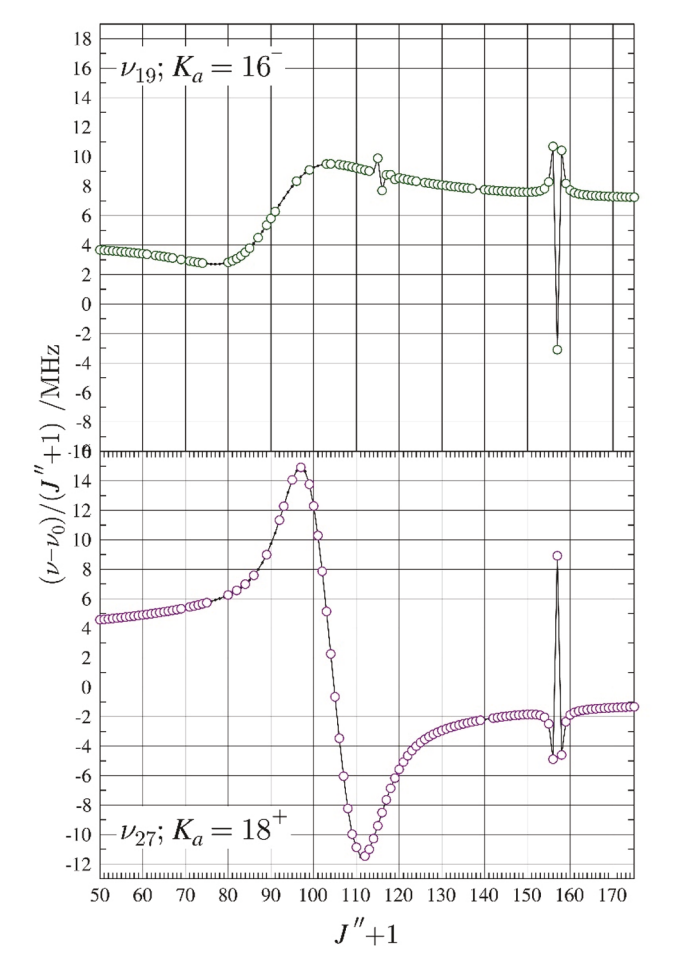


Fig. 8. Resonance plots for cyanopyrazine showing the $K_a=16^-$ series for ν_{19} and $K_a=18^+$ series for ν_{27} . These two resonances conform to the $\Delta K_a=2$ selection rule for a-type resonances. The plotted values are frequency differences between excited-state transitions and their ground-state counterparts, scaled by (J''+1) in order to make the plots more horizontal. Measured transitions are represented by circles: ν_{27} (purple), ν_{19} (green). Predictions from the final coupled fit are represented by a solid, colored line. (For interpretation of the references to colour in this figure legend, the reader is referred to the web version of this article.)

work.

Two additional types of transitions are observed in the excited-state spectra of cyanopyrazine that are made possible by the coupling of the fundamental states: b-type transitions that are more intense than they would be due purely to the b-axis dipole moment and nominal interstate transitions. As observed with cyanocyclobutene [41], the state mixing of ν_{27} and ν_{19} allows intensity transfer from a-type transitions to b-type transitions. In this case, b-type transitions are observed for each vibrationally excited state, unlike cyanocyclobutene where they were only observed in v_{17} . The result is that there are many b-type, R-branch transitions assigned, measured, and least-squares fit for the dyad despite the very small μ_b (approximately 42 times smaller than μ_a). Formally forbidden, nominal interstate rotational transitions are observable from the energy levels with the most intense state-mixing. They share at least one energy level with a transition involved in a resonance and borrow intensity from those resonant transitions. In some cases, the intensity borrowing is so profound that the intrastate resonant transitions have vanishingly small intensities and cannot be observed. In other cases, such as the one highlighted in Fig. 10, all four transitions (two intrastate resonant transitions and two interstate transitions) can be observed and included in the least-squares fit. Since the four transitions involve the same four energy levels, the average of the nominal interstate frequencies should be the same as that of the intrastate frequencies. For the particular set depicted in Fig. 10, the averages differ by only 25 kHz, giving confidence in their assignment and in the dyad least-squares fit overall. The inclusion of the many b-type transitions and the nominal interstate transitions provides a substantial constraint on the $\Delta E_{27,19}$ value and Coriolis-coupling constants. As a result, we are confident that the spectroscopic constants provided are well-determined and likely to be physically meaningful and predictive beyond the studied frequency range.

5. Conclusion

The transition frequencies and spectroscopic constants for cyanopyrazine, presented in this work, provide the necessary laboratory data for future astronomical searches for this potential pyrazine tracer. Combined with computed or experimental nuclear quadrupole coupling constants, the spectroscopic constants should reliably predict transition frequencies to much lower or slightly higher frequencies for the ground and two lowest-energy fundamental states. While this work provides the precise and accurate energy separation between vibrational modes ν_{27} and ν_{19} , high-resolution infrared spectroscopy or other spectroscopy that would provide a direct measurement of the frequency of either v_{27} or ν_{19} is needed to determine both fundamental frequencies. This measurement would be somewhat challenging due to the low predicted IR intensities of ν_{27} and ν_{19} (1.5 and 0.4 km/mol, respectively; MP2). Such an investigation would also resolve the ambiguity concerning the proper assignment of these two modes from the previous low-resolution infrared study. A high-resolution infrared study would further provide the necessary information to begin to address the complex set of interacting vibrationally excited states higher in energy than ν_{27} and ν_{19} . The two-quanta states of ν_{27} and ν_{19} are expected to form a complicated tetrad of states with ν_{26} (0.8 km/mol, MP2), as shown in Fig. 6. Although the millimeter-wave intensities of these transitions are expected to be strong enough to readily observe their spectra, and many perturbation constants can be predicted by scaling the coupling constants between ν_{27} and v_{19} by a factor of $\sqrt{2}$, achieving a satisfactory least-squares fit will still be a challenging endeavor.

Declaration of Competing Interest

The authors declare that they have no known competing financial interests or personal relationships that could have appeared to influence the work reported in this paper.

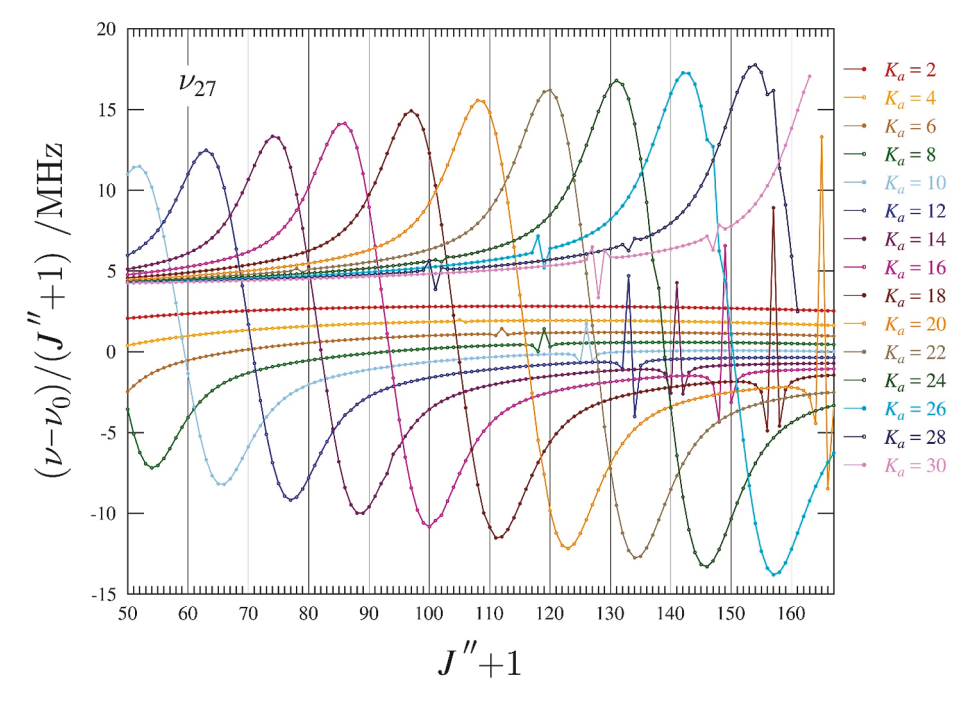
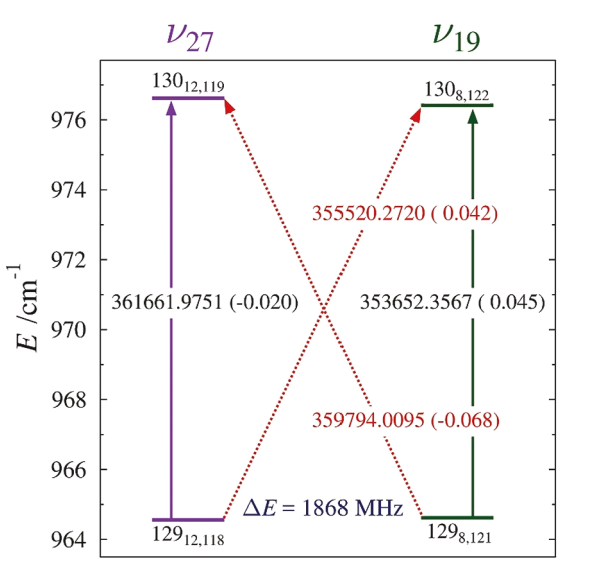


Fig. 9. Superimposed resonance plots of ν_{27} for ${}^aR_{0,1}$ even- K_a^+ series from 2 to 30 for cyanopyrazine. Measured transitions are omitted for clarity, but they are indistinguishable from the plotted values on this scale. The plotted values are frequency differences between excited-state transitions and their ground-state counterparts, scaled by (J'' + 1).



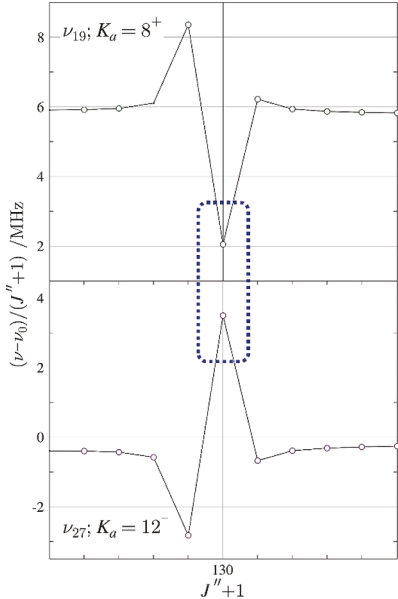


Fig. 10. Energy diagram (left) depicting a representative matched pair of nominal interstate transitions between the ν_{27} (purple) and ν_{19} (dark green) vibrational states of cyanopyrazine. Standard ^aR_{0.1} transitions within vibrational states are denoted by vertical arrows. The diagonal, dashed arrows indicate nominal interstate transitions that are formally forbidden, but enabled as a result of rotational energy-level mixing. The value printed on each of the arrows is the corresponding transition frequency (in MHz) with its obs. - calc. value in parentheses. The marked energy separation is between the two strongly interacting rotational energy levels. Resonance plots (right) of the K_a series of ν_{27} and ν_{19} that contain the corresponding resonant transitions, which are identified with a blue box. (For interpretation of the references to colour in this figure legend, the reader is referred to the web version of this article.)

Data availability

Data will be made available on request.

Acknowledgments

We gratefully acknowledge funding from the U.S. National Science Foundation for support of this project (CHE-1664912 and CHE-1954270). We thank Michael McCarthy for the loan of an amplification-multiplication chain and the Harvey Spangler Award (to B.J.E.) for support of the purchase of the corresponding zero-bias detector.

Appendix A. Supplementary material

Supplementary data to this article can be found online at https://doi.org/10.1016/j.jms.2022.111703.

References

- J. Cernicharo, A.M. Heras, A.G.G.M. Tielens, J.R. Pardo, F. Herpin, M. Guélin, L.B. F.M. Waters, Infrared Space Observatory's Discovery of C₄H₂, C₆H₂, and Benzene in CRL 618, Astrophys. J. 546 (2) (2001) L123–L126.
- [2] S.T. Ridgway, D.N.B. Hall, S.G. Kleinmann, D.A. Weinberger, R.S. Wojslaw, Circumstellar acetylene in the infrared spectrum of IRC +10° 216, Nature 264 (5584) (1976) 345–346.

- [3] B.A. McGuire, A.M. Burkhardt, S.V. Kalenskii, C.N. Shingledecker, A.J. Remijan, E. Herbst, M.C. McCarthy, Detection of the Aromatic Molecule Benzonitrile (c-C₆H₅CN) in the Interstellar Medium, Science 359 (6372) (2018) 202 205.
- [4] B.A. McGuire, A. Loomis Ryan, A.M. Burkhardt, K. Lee Kin Long, C. N. Shingledecker, S.B. Charnley, I.R. Cooke, M.A. Cordiner, E. Herbst, S. Kalenskii, M.A. Siebert, E.R. Willis, C. Xue, A.J. Remijan, M.C. McCarthy, Detection of two interstellar polycyclic aromatic hydrocarbons via spectral matched filtering, Science 371 (6535) (2021) 1265 1269.
- [5] M.C. McCarthy, B.A. McGuire, Aromatics and Cyclic Molecules in Molecular Clouds: A New Dimension of Interstellar Organic Chemistry, J. Phys. Chem. A 125 (16) (2021) 3231–3243.
- [6] H.S.P. Müller, F. Schlöder, J. Stutzki, G. Winnewisser, The Cologne Database for Molecular Spectroscopy, CDMS: a Useful Tool for Astronomers and Spectroscopists, J. Mol. Struct. 742 (1 3) (2005) 215–227.
- [7] H.S.P. Müller, S. Thorwirth, D.A. Roth, G. Winnewisser, The Cologne Database for Molecular Spectroscopy, CDMS, Astron. Astrophys. 370 (3) (2001) L49 L52.
- [8] M.A. Zdanovskaia, B.J. Esselman, H.S. Lau, D.M. Bates, R.C. Woods, R.J. McMahon, Z. Kisiel, The 103 360 GHz rotational spectrum of benzonitrile, the first interstellar benzene derivative detected by radioastronomy, J. Mol. Spectrosc. 351 (2018) 39 48.
- [9] M.A. Zdanovskaia, M.-A. Martin-Drumel, Z. Kisiel, O. Pirali, B.J. Esselman, R. C. Woods, R.J. McMahon, The eight lowest-energy vibrational states of benzonitrile: analysis of Coriolis and Darling-Dennison couplings by millimeter-wave and far-infrared spectroscopy, J. Mol. Spectrosc. 383 (2022), 111568.
- [10] P.M. Dorman, B.J. Esselman, R.C. Woods, R.J. McMahon, An analysis of the rotational ground state and lowest-energy vibrationally excited dyad of 3-cyanopyridine: Low symmetry reveals rich complexity of perturbations, couplings, and interstate transitions, J. Mol. Spectrosc. 373 (2020), 111373.
- [11] P.M. Dorman, B.J. Esselman, J.E. Park, R.C. Woods, R.J. McMahon, Millimeter-wave spectrum of 4-cyanopyridine in its ground state and lowest-energy vibrationally excited states, 20 and 30, J. Mol. Spectrosc. 369 (2020), 111274.
- [12] D. McNaughton, M.K. Jahn, M.J. Travers, D. Wachsmuth, P.D. Godfrey, J.-U. Grabow, Laboratory rotational spectroscopy of cyano substituted polycyclic aromatic hydrocarbons, Mon. Not. R. Astron. Soc. 476 (4) (2018) 5268-5273.
- [13] P.M. Dorman, B.J. Esselman, R.C. Woods, R.J. McMahon, Unpublished work, 2022.
- [14] H.H. Smith, B.J. Esselman, R.C. Woods, R.J. McMahon, Unpublished work, 2022.
- [15] W. Werner, H. Dreizler, H.D. Rudolph, Zum Mikrowellenspektrum des Pyridazins, Z. Naturforsch. A 22 (4) (1967) 531 543.
- [16] G.L. Blackman, R.D. Brown, F.R. Burden, The microwave spectrum, dipole moment, and nuclear quadrupole coupling constants of pyrimidine, J. Mol. Spectrosc. 35 (3) (1970) 444 454.
- [17] T.J. Barnum, M.A. Siebert, K.L.K. Lee, R.A. Loomis, P.B. Changala, S.B. Charnley, M.L. Sita, C. Xue, A.J. Remijan, A.M. Burkhardt, B.A. McGuire, I.R. Cooke, A Search for Heterocycles in GOTHAM Observations of TMC-1, J. Phys. Chem. A 126 (17) (2022) 2716 2728.
- [18] E.E. Etim, R.O.A. Adelagun, C. Andrew, O. Enock Oluwole, Optimizing the searches for interstellar heterocycles, Adv. Space Res. 68 (8) (2021) 3508–3520.
- [19] S.B. Charnley, Y.-J. Kuan, H.-C. Huang, O. Botta, H.M. Butner, N. Cox, D. Despois, P. Ehrenfreund, Z. Kisiel, Y.-Y. Lee, A.J. Markwick, Z. Peeters, S.D. Rodgers, Astronomical searches for nitrogen heterocycles, Adv. Space Res. 36 (2) (2005) 137–145.
- [20] Y.-J. Kuan, C.-H. Yan, S.B. Charnley, Z. Kisiel, P. Ehrenfreund, H.-C. Huang, A search for interstellar pyrimidine, Mon. Not. R. Astron. Soc. 345 (2003) 650–656.
- [21] M. Nabavian, R. Sabbah, R. Chastel, M. Laffitte, Thermodynamique de composés azotés-II. Étude thermochimique des acides aminobenzoïques, de la pyrimidine, de l uracile et de la thymine, J. Chim. Phys. 74 (1977) 115 126.
- [22] J. Tjebbes, The heats of combustion and formation of the three diazines and their resonance energies, Acta Chem. Scand. 16 (4) (1962) 916 921.
- [23] Z.N. Heim, B.K. Amberger, B.J. Esselman, J.F. Stanton, R.C. Woods, R.J. McMahon, Molecular structure determination: Equilibrium structure of pyrimidine (m-C₄H₄N₂) from rotational spectroscopy ($r_e^{\rm SE}$) and high-level ab initio calculation (r_e) agree within the uncertainty of experimental measurement, J. Chem. Phys. 152 (10) (2020), 104303.

- [24] S. Akavipat, C.F. Su, R.L. Cook, Microwave spectra of chloropyrazine, J. Mol. Spectrosc. 111 (1) (1985) 209 210.
- [25] P.M. Higgins, B.J. Esselman, M.A. Zdanovskaia, R.C. Woods, R.J. McMahon, Millimeter-wave spectroscopy of the chlorine isotopologues of chloropyrazine and twenty-two of their vibrationally excited states, J. Mol. Spectrosc. 364 (2019), 111179.
- [26] F.B. Mortzfeld, C. Hashem, K. Vranková, M. Winkler, F. Rudroff, Pyrazines: Synthesis and Industrial Application of these Valuable Flavor and Fragrance Compounds, Biotechnol. J. 15 (11) (2020) 2000064.
- [27] B.K. Amberger, B.J. Esselman, J.F. Stanton, R.C. Woods, R.J. McMahon, Precise Equilibrium Structure Determination of Hydrazoic Acid (HN₃) by Millimeter-wave Spectroscopy, J. Chem. Phys. 143 (10) (2015), 104310.
- [28] B.J. Esselman, B.K. Amberger, J.D. Shutter, M.A. Daane, J.F. Stanton, R.C. Woods, R.J. McMahon, Rotational Spectroscopy of Pyridazine and its Isotopologs from 235 360 GHz: Equilibrium Structure and Vibrational Satellites, J. Chem. Phys. 139 (2013), 224304.
- [29] Z. Kisiel, L. Pszczó kowski, B.J. Drouin, C.S. Brauer, S. Yu, J.C. Pearson, I. R. Medvedev, S. Fortman, C. Neese, Broadband rotational spectroscopy of acrylonitrile: Vibrational energies from perturbations, J. Mol. Spectrosc. 280 (2012) 134 144.
- [30] Z. Kisiel, L. Pszczó kowski, I.R. Medvedev, M. Winnewisser, F.C. De Lucia, E. Herbst, Rotational spectrum of *trans trans* diethyl ether in the ground and three excited vibrational states, J. Mol. Spectrosc. 233 (2) (2005) 231 243.
- [31] H.M. Pickett, The fitting and prediction of vibration-rotation spectra with spin interactions, J. Mol. Spectrosc. 148 (2) (1991) 371 377.
- [32] Z. Kisiel, PROSPE Programs for ROtational SPEctroscopy, 2020. http://info.ifpan.edu.pl/~kisiel/prospe.htm. (Accessed 07-11-2020.
- [33] M.J. Frisch, G.W. Trucks, H.B. Schlegel, G.E. Scuseria, M.A. Robb, J.R. Cheeseman, G. Scalmani, V. Barone, G.A. Petersson, H. Nakatsuji, X. Li, M. Caricato, A.V. Marenich, J. Bloino, B.G. Janesko, R. Gomperts, B. Mennucci, H.P. Hratchian, J.V. Ortiz, A.F. Izmaylov, J.L. Sonnenberg, D. Williams-Young, F. Ding, F. Lipparini, F. Egidi, J. Goings, B. Peng, A. Petrone, T. Henderson, D. Ranasinghe, V.G. Zakrzewski, J. Gao, N. Rega, G. Zheng, W. Liang, M. Hada, M. Ehara, K. Toyota, R. Fukuda, J. Hasegawa, M. Ishida, T. Nakajima, Y. Honda, O. Kitao, H. Nakai, T. Vreven, K. Throssell, J.A. Montgomery, Jr., J.E. Peralta, F. Ogliaro, M.J. Bearpark, J.J. Heyd, E.N. Brothers, K.N. Kudin, V.N. Staroverov, T.A. Keith, R. Kobayashi, J. Normand, K. Raghavachari, A.P. Rendell, J.C. Burant, S.S. Iyengar, J. Tomasi, M. Cossi, J.M. Millam, M. Klene, C. Adamo, R. Cammi, J.W. Ochterski, R.L. Martin, K. Morokuma, O. Farkas, J.B. Foresman, D.J. Fox, Gaussian 16 rev C.01, Gaussian, Inc., Wallingford, CT, USA, 2016.
- [34] J.R. Schmidt, W.F. Polik, WebMO Enterprise, version 19.0; WebMO LLC: Madison, WI, USA, 2019; http://www.webmo.net (accessed August, 2019).
- [35] M.A. Zdanovskaia, B.J. Esselman, R.C. Woods, R.J. McMahon, The 130 370 GHz rotational spectrum of phenyl isocyanide (C₆H₅NC), J. Chem. Phys. 151 (2) (2019), 024301.
- [36] H. Shindo, Studies on the Infrared Spectra of Heterocyclic Compound. VIII. Infrared Spectra of Substituted Pyrazines and their N-Oxides, Chem. Pharm. Bull. 8 (1) (1960) 33 45.
- [37] J. Bus, T.J. Liefkens, W. Schwaiger, Infrared spectrometry of pyrazines, Recl. Trav. Chim. Pays-Bas 92 (1) (1973) 123 126.
- [38] M.J.M. Delgado, F. Márquez, M.I. Suero, J.I. Marcos, Vibrational spectra of pyrazincarbonitrile and [15N]pyrazincarbonitrile, J. Raman Spectrosc. 20 (2) (1989) 63 65.
- [39] K.V. Shuvaev, T.S.M. Abedin, C.A. McClary, L.N. Dawe, J.L. Collins, L. K. Thompson, Ligand directed self-assembly vs. metal ion coordination algorithm when does the ligand or the metal take control? Dalton Trans. 16 (2009) 2926–2939.
- [40] B.J. Esselman, S.M. Kougias, M.A. Zdanovskaia, R.C. Woods, R.J. McMahon, Synthesis, Purification, and Rotational Spectroscopy of (Cyanomethylene) Cyclopropane An Isomer of Pyridine, J. Phys. Chem. A 125 (25) (2021) 5601 5614.
- [41] H.H. Smith, S.M. Kougias, B.J. Esselman, R.C. Woods, R.J. McMahon, Synthesis, Purification, and Rotational Spectroscopy of 1-Cyanocyclobutene (C₅H₅N), J. Phys. Chem. A 126 (12) (2022) 1980 1993.